

# Topological Quantum Phase Transitions Retrieved from Manifold Learning

Yanming Che,<sup>1,\*</sup> Clemens Gneiting,<sup>1</sup> Tao Liu,<sup>1</sup> and Franco Nori<sup>1,2,†</sup>

<sup>1</sup>*Theoretical Quantum Physics Laboratory, RIKEN Cluster for Pioneering Research, Wako-shi, Saitama 351-0198, Japan*

<sup>2</sup>*Department of Physics, The University of Michigan, Ann Arbor, Michigan 48109-1040, USA*

(Dated: March 27, 2025)

The discovery of topological features of quantum states plays a central role in modern condensed matter physics and various artificial systems. Due to the absence of local order parameters, the detection of topological quantum phase transitions (TQPTs) remains a challenge. Machine learning may provide effective methods for identifying topological features. In this work, we show that manifold learning can successfully retrieve TQPTs in momentum space. Our results show that the Chebyshev distance (CD) between two data points can successfully capture the main features of TQPTs, while the widely used Euclidean distance in general *fails*. The similarity matrix built upon the CD thus naturally exhibits uncorrelated cluster structures, corresponding to distinct sectors in the topological phase diagram. Then a diffusion map is applied to implement dimensionality reduction and to learn about TQPTs in an unsupervised manner. Our demonstrations on the Su-SchriefferHeeger (SSH) model, the 2D Qi-Wu-Zhang (QWZ) model, and the quenched SSH model show the capability of generic unsupervised learning, when equipped with a suitable distance metric, in exploring TQPTs.

*Introduction.*—Topological phases of matter have attracted tremendous attention in the past decade [1–5]. Conceptually, topological quantum phase transitions (TQPTs) go beyond the conventional Landau paradigm, which needs local order parameters to distinguish different phases. Instead, topological quantum phases are usually characterized by topological quantum numbers, which reflect global properties of the state manifold defined on a compact Brillouin zone (BZ). Quantum states belonging to the same topological sector can be continuously deformed to each other without closing the bulk energy gap, and are thus called homotopic. When a TQPT occurs, according to the bulk-boundary correspondence, the band gap closes at the critical point. Therefore, a TQPT is usually accompanied by a discontinuous change of the state configuration, such as the sign change of the mass term in the Hamiltonian, or band inversions in topological insulators [1, 2].

Due to the absence of local order parameters, the detection of TQPTs remains a challenge. For a given Hamiltonian in momentum space featuring a set of parameters, it is usually not obvious whether it exhibits TQPTs when sweeping the parameters. Recently, machine learning methods have been successfully used to detect phase transitions in topological systems [6–13] and many-body physics [14–25]. In particular, deep learning has been employed [7] to train a neural network (NN) to recognize different winding numbers of one-dimensional spin systems in a supervised manner. However, prior knowledge and labeled training examples are not always easily accessible in practice. In that respect, the unsupervised learning, without pre-training, provides a more promising learning framework to discover topological patterns. For instance, NNs with autoencoders [26] and predictive models [13] were used to learn topological features without explicit supervisions. Compared

with deep learning, manifold learning methods, such as Isomaps [27] and diffusion maps [28, 29], usually require lower computational costs. The unsupervised learning based on diffusion maps has been successfully applied for the identification of topological clusters [12]. The application of this method leaves the freedom to choose the distance metric in the original feature space. The Euclidean distance (ED), which has been used in most cases, appears as a natural choice.

In this Letter, we argue that, in the context of identifying TQPTs in momentum space, the ED may be suboptimal, while the Chebyshev distance (CD) prevails in many relevant cases. This is because, as mentioned above, the Hamiltonian or ground state of a quantum system defined in momentum space undergoes rapid changes at specific points in the BZ when the system goes across the topological critical point. The CD highlights these features of TQPTs and is thus a more suitable approximation of the homotopic distance than the ED. Motivated by manifold learning methods, we explore non-Euclidean structures of topological data vectors that are uniformly sampled from the Hamiltonian parameter space. With the CD as a distance metric in the feature space, TQPTs of the two-dimensional (2D) Qi-Wu-Zhang (QWZ) model [30], the Su-SchriefferHeeger (SSH) model, and the (1 + 1)-dimensional quenched SSH model [31] are uncovered, respectively. Our results highlight the capability and promising performance of unsupervised machine learning of TQPTs without prior analysis of the Hamiltonian.

*Manifold learning and distance metric.*—Manifold learning is used when linear unsupervised learning models, like principle components analysis (PCA), fail to uncover nonlinear structures in data sets [27, 32]. A key characteristic of manifold learning methods such as Isomap [27] is that the ED is not suitable to reflect the intrinsic connectivity and similarity between data points.

<sup>\*</sup>Correspondence to: cgeiting@umich.edu

<sup>†</sup>Correspondence to: nori@riken.jp

Adapted distance metrics, such as the manifold geodesic distance, should then be used to characterize the similarities.

When it comes to the unsupervised learning of TQPTs for states in momentum space, one comes across a similar problem: *the ED in general cannot successfully retrieve topological clusters in the data set*. A homotopic distance metric (see e.g., Ref. [33]) is instead needed to adequately capture the topological structure of the data set. While the generic numerical evaluation of the homotopic distance between two input vectors is difficult at the current stage, some approximative metrics may be used. Motivated by the observation that topological transitions usually are accompanied by *sign changes or band inversions*, here we investigate the use of the  $\mathbb{L}^\infty$ -norm induced CD to (approximately) measure topological similarities. Across topological transitions, quantum states defined over the compact BZ take sharp changes at certain symmetric points in the BZ [34], while state vectors belonging to the same topological phase vary smoothly. The CD *highlights* these features of TQPTs, facilitating the learning of TQPTs.

To see this more clearly, we analyze the performance of the distance metric in clustering with the similarity matrix

$$\mathcal{K}_{ij}^p = \exp\left(-\frac{\|\mathbf{x}_i - \mathbf{x}_j\|_{\mathbb{L}^p}^2}{\epsilon}\right), \quad (1)$$

where  $\epsilon$  is the resolution parameter of the kernel,  $\mathbf{x}_i$  is the  $i$ th input data vector and  $i, j = 0, 1, 2, \dots, M-1$ , with  $M$  the size of the data set. The  $\mathbb{L}^p$  norm of vector  $\mathbf{z}$  is given by  $\|\mathbf{z}\|_{\mathbb{L}^p} = (\sum_k z_k^p)^{1/p}$ , where  $p = 2$  and  $p = \infty$  give the ED and the CD, respectively [35]. An equivalent but more useful expression for the  $\mathbb{L}^\infty$  norm is  $\|\mathbf{z}\|_{\mathbb{L}^\infty} = \max_k |z_k|$ . For comparison, we show the similarity matrix  $\mathcal{K}^p$  built upon the CD in Fig. 1(a) and upon the ED in Fig. 1(b) for the 2D QWZ model [30] [see Eq. (2)]. The data points are uniformly sampled in an ordered way such that one can see four equally partitioned clusters. The resolution parameters are optimized with respect to the ideal similarity matrix (see the caption of Fig. 1 for details). Compared to the ED displayed in Fig. 1(b), the similarity matrix from the CD in Fig. 1(a) clearly shows four nearly ideal clusters with good (poor) intra- (inter-) cluster connectivity, which correspond to four distinct sectors in the topological phase diagram in Fig. 2(a). The ED leads to connected clusters, and we find that, even for smaller values of  $\epsilon$ , the first two sectors with the ED are connected and thus cannot be correctly clustered by the diffusion-map algorithm.

*Diffusion map and dimensionality reduction.*—With the CD as a topologically viable distance measure, we are now ready to seek an appropriate approach for the dimensionality reduction, to learn the topological clusters. Among many manifold learning methods [27, 32, 36–38], diffusion maps [12, 28, 29, 39–41] can successfully

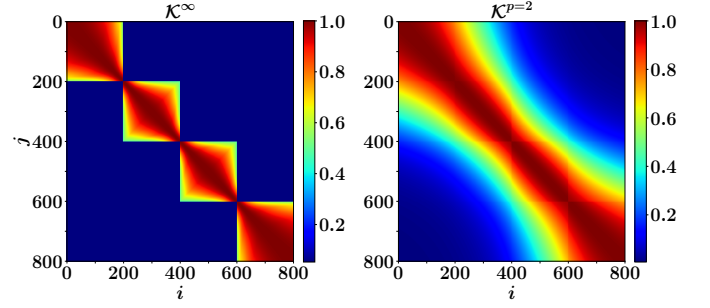


Figure 1. (Color online) Similarity matrix  $\mathcal{K}^p$  in Eq. (1) built from the  $\mathbb{L}^p$ -norm distance metric: Compared are the (a) Chebyshev distance (CD) with  $p = \infty$  and (b) the Euclidean distance (ED) with  $p = 2$ .  $M = 800$  input data points are uniformly sampled in an *ordered* manner, from the 2D QWZ model in Eq. (2), where the hopping energy is taken to be  $b = 0.2$  and the chemical potential  $\mu$  varies from  $\mu = -4b$  to  $\mu = 12b$ , and the BZ is sliced into  $32 \times 32$  patches. Compared to (b), (a) shows four nearly ideal clusters with good (poor) intra- (inter-) cluster connectivity (corresponding four squares in the diagonal direction). The resolution parameters are  $\epsilon = 0.34$  in (a) and  $\epsilon = 1.27 \times 10^{-4}$  in (b), which are obtained by minimizing the respective mean square errors (MSEs) with respect to the ideal similarity matrix, where matrix elements for intra-cluster data points equal one and equal zero for the others.

discover the connected components in a data manifold if a viable distance measure is used, visualized by the similarity matrix in Fig. 1. In the framework of diffusion maps, a Markovian random walk is launched within the data set, where the transition probability between two data points is given by the normalized similarity matrix,  $P_{ij} = \mathcal{K}_{ij}^p / \sum_j \mathcal{K}_{ij}^p$ . After  $t$  steps of random walk, the connectivity between two points  $\mathbf{x}_i$  and  $\mathbf{x}_j$  is characterized by the diffusion distance,  $D_t^2(\mathbf{x}_i, \mathbf{x}_j) = \sum_k [(P^t)_{ik} - (P^t)_{jk}]^2 / \phi_0(\mathbf{x}_k)$ , where  $\phi_0(\mathbf{x}_k)$  is the first left eigenvector of  $P$  [39]. The map to the Euclidean space  $Y$ , which best preserves the connectivity of the data set, is determined by minimizing the cost function [36]  $C = \sum_{ij} [D_t(\mathbf{x}_i, \mathbf{x}_j) - d_Y(\mathbf{y}_i, \mathbf{y}_j)]^2$ , where  $d_Y(\mathbf{y}_i, \mathbf{y}_j)$  is the  $Y$ -space Euclidean distance between the images  $\mathbf{y}_i$  and  $\mathbf{y}_j$  of two data points. The solution of minimizing the above cost function is given by [39]  $\mathbf{y}_i = [\lambda_0^t \psi_0(\mathbf{x}_i), \lambda_1^t \psi_1(\mathbf{x}_i), \dots, \lambda_{M-1}^t \psi_{M-1}(\mathbf{x}_i)]$ , where  $\lambda_k$  and  $\psi_k(\mathbf{x}_i)$  are the  $k$ th eigenvalue and the right eigenvector's  $i$ th component of the  $P^t$  matrix, respectively [42]. Statistics and clustering methods such as  $k$ -means will be used in the  $Y$  space to identify the samples in each cluster, and the critical lines are decided *automatically* by the corresponding cluster boundaries in the parameter space.

*Learning TQPTs in 2D.*—First we consider the QWZ model in 2D [30]. The Hamiltonian in momentum space is  $H(\mathbf{k}) = d_0(\mathbf{k}) + \mathbf{d}(\mathbf{k}) \cdot \boldsymbol{\sigma}$ , with  $\boldsymbol{\sigma} = (\sigma_x, \sigma_y, \sigma_z)$  the vector of Pauli matrices and  $\mathbf{d}(\mathbf{k})$  a three-dimensional

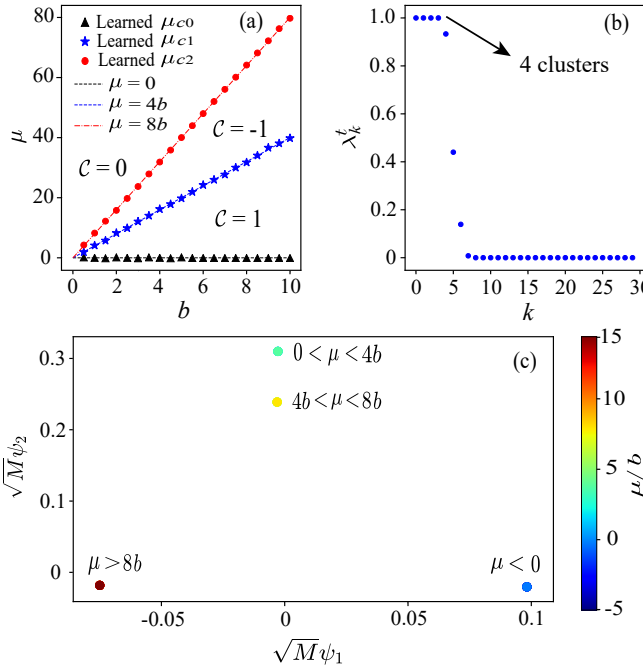


Figure 2. (a) TQPTs of the QWZ model from unsupervised learning. The critical lines are automatically learned by scanning the hopping energy  $b$  and for each value of  $b$ , the input data set consists of sampled feature vectors from  $\mu = -5b$  to  $\mu = 15b$ . The critical values of the chemical potential  $\mu$  are identified by  $k$ -means in the diffusion space from the boundaries of  $\mu$  parameters in each cluster. The first topologically trivial phase with  $\mu < 0$  and  $\mathcal{C} = 0$  is not shown. (b) First 30 eigenvalues of the diffusion matrix  $P^t$ . The degeneracy of the largest  $\lambda_k^t$  indicates that there are 4 disconnected clusters in total. (c) Images of the data set in the low-dimensional diffusion space. The clustering is very effective such that the size of each cluster is far smaller than their diffusion distance. The color code indicates different values of  $\mu/b$ . (b) and (c) are plotted with a representative value of  $b = 1$ . The parameters used are  $M = 1000$ ,  $N = 32$ ,  $\epsilon = 0.03$ , and  $t = 500$ . *In contrast, the use of the ED does not deliver the correct clustering, independent of the choice of  $\epsilon$ .*

vector with components

$$\begin{aligned} d_x &= \sin(k_x), & d_y &= \sin(k_y), \\ d_z &= \mu - 2b[2 - \cos(k_x) - \cos(k_y)], \end{aligned} \quad (2)$$

where  $\mu$  is the chemical potential and  $b$  is the hopping energy, and we have taken a unit lattice constant. The 2D BZ is given by  $[-\pi, \pi] \times [-\pi, \pi]$ . We can further assume  $d_0(\mathbf{k}) = 0$ , because it trivially contributes to the topology. The normalized unit vector  $\hat{\mathbf{d}}(\mathbf{k}) = \mathbf{d}(\mathbf{k}) / |\mathbf{d}(\mathbf{k})|$  defines a mapping from the compact 2D BZ (i.e.,  $\mathbb{T}^2$ ) to the unit sphere  $\mathbb{S}^2$ . The topological Chern number  $\mathcal{C}_{2D} = \frac{1}{4\pi} \int_{BZ} dk_x dk_y \hat{\mathbf{d}} \cdot (\partial_{k_x} \hat{\mathbf{d}} \times \partial_{k_y} \hat{\mathbf{d}})$  measures how many times the mapping wraps over the unit sphere.

Shown in Fig. 2(a) are the topological critical lines *automatically* learned in an unsupervised manner by scanning through the hopping energy  $b$ . For fixed  $b$ , the

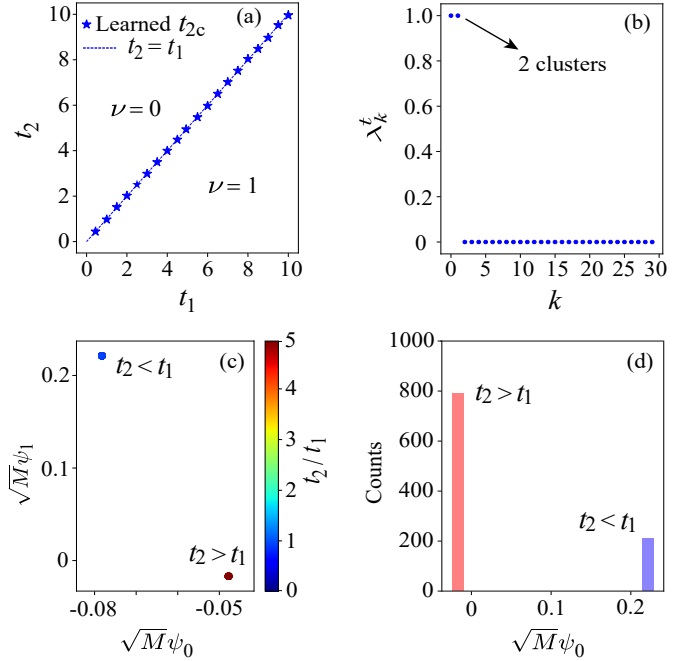


Figure 3. (a) Learned TQPT of the SSH model. The critical line is automatically learned by scanning the hopping energy parameter  $t_1$  and for each  $t_1$ , the input data set is composed of uniformly sampled feature vectors from  $t_2 \in (0, 5t_1]$ . There are only two topological sectors detected, as illustrated by the degree of degeneracy of the largest eigenvalue  $\lambda_k^t$  in (b). (c) Images of the data set in the diffusion space. The clustering is very successful where the size of each cluster is far smaller than their inter distance. The color values shows different values of  $t_2/t_1$ . (b) and (c) are plotted with a representative value of  $t_1 = 1$ . Other parameters used are  $M = 1000$ ,  $N = 32$ ,  $\epsilon = 0.03$ , and  $t = 500$ .

data set consists of  $M$  uniformly sampled  $\hat{\mathbf{d}}$  vectors from  $\mu = -5b$  to  $\mu = 15b$ , and  $\hat{\mathbf{d}}(\mathbf{k})$  is vectorized to a high-dimensional feature vector in  $\mathbb{R}^{3(N+1)^2}$ , where we have discretized the BZ into  $N \times N$  patches. The learned black triangles, red dots and blue stars precisely trace three critical lines that divide the parameter  $(\mu, b)$  space into four topological sectors. It should be noted that *further topological information* may be retrieved from Fig. 1(a), where the first and fourth, the second and third clusters are quasi-symmetric, respectively; indicating that the corresponding two sectors in the phase diagram may have related topology. This can be verified by calculating the Chern numbers within each phase, as shown in Fig. 2(a). The number of degenerate eigenvalues with  $\lambda_k^t \approx 1$  in Fig. 2(b) determines the number of distinct topological sectors. Fig. 2(c) shows the data set embedded in the diffusion space. The size of each cluster is sufficiently small such that points belonging to the same sector almost collapse. Compared to supervised learning, here the learning is automatically achieved without prior training.

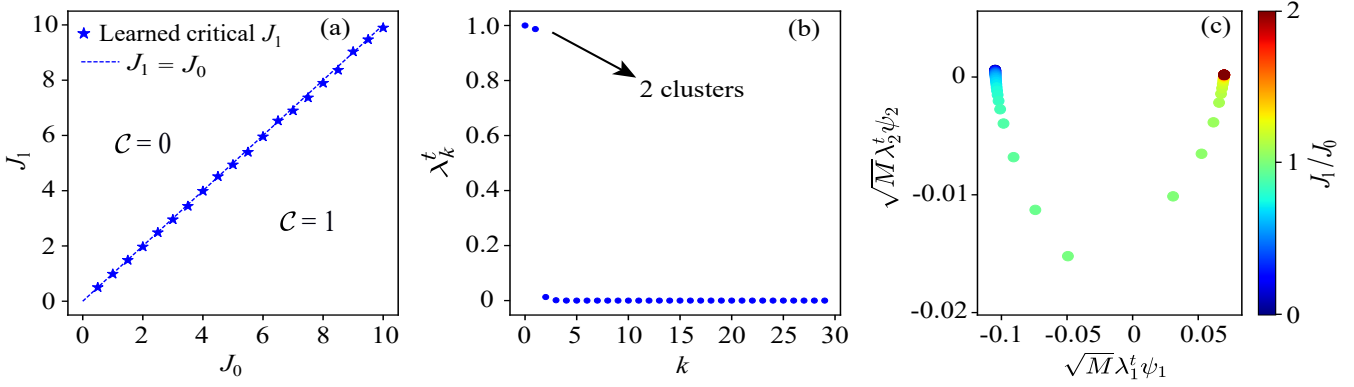


Figure 4. (a) TQPT of a quenched SSH model, retrieved with unsupervised learning. Only two topological sectors are detected. The transition line is automatically learned by varying the parameter  $J_0$ , and for each fixed value of  $J_0$  our input data set consists of sampled feature vectors from  $J_1 \in (0, 2J_0]$ . (b) shows the first 20 eigenvalues  $\lambda_k^t$  with  $t = 100$ . The number of (near) degenerate largest eigenvalues indicate that there are two topological sectors. (c) Images of the data set in the embedded low-dimensional flat space. The  $k$ -means clustering method is used to automatically identify each cluster and the corresponding parameter  $J_1$  for each data point. The critical line in (a) is obtained from the identified  $J_1$  boundaries in each cluster. The color code indicates different values of  $J_1/J_0$ . (b) and (c) are plotted with a representative value of  $J_0 = 1$ . Here we have used  $M = 1000$ ,  $N = 32$ ,  $\epsilon = 0.03$ .

*Learning the SSH model.*—The SSH model describes electrons in an one-dimensional lattice [43, 44], with  $t_1$  and  $t_2$  the staggered hopping energies. The Hamiltonian of the SSH model in momentum space reads  $H(k) = [t_1 + t_2 \cos(k)] \sigma_x + t_2 \sin(k) \sigma_y$ . In the Bloch vector formulation as in the 2D case, we have  $d_x(k) = [t_1 + t_2 \cos(k)]$ ,  $d_y(k) = t_2 \sin(k)$  and  $d_z = 0$ . Note that the absence of the third component is related to the chiral symmetry of the SSH Hamiltonian. The unit vector  $\mathbf{d}(k) = \mathbf{d}(k) / |\mathbf{d}(k)|$  defines a map  $\hat{\mathbf{d}}(k) : S^1 \mapsto S^1$ , where the topological winding number is [44]  $\nu = \frac{1}{2\pi i} \int_{-\pi}^{\pi} dk q^{-1}(k) \partial_k q(k)$ , with  $q(k) = d_x(k) - id_y(k)$ . The input data is given by the reshaped  $\hat{\mathbf{d}}(k)$  ( $k \in \text{BZ}$ ) vector in high-dimensional feature space  $\mathbb{R}^{2(N+1)}$ , after slicing the BZ into  $N$  patches. For fixed  $t_1$ , the data set is obtained from uniformly sampled feature vectors from  $t_2 = 0$  to  $t_2 = 5t_1$ . Shown in Fig. 3(a) is the learned phase diagram indicating that there are only two topologically distinct sectors (also indicated in Fig. 3(b) by the degeneracy of  $\lambda^t$  with a large  $t$ ). The topological winding numbers are calculated according to the above winding-number formula. Figs. 3(c)-(d) show the distribution of data points in the low-dimensional diffusion space. The critical line in Fig. 3(a) is decided by fixing  $t_1$  and identifying the  $t_2$  parameters in each topological cluster in Fig. 3(c). The obtained TQPT coincides with the theoretical prediction [44].

*Learning topological phases of the quenched SSH model.*—As a final demonstration, we provide the unsupervised learning of the dynamically quenched SSH model [31]. Here the hopping energies  $(t_1, t_2) = (J_0, 0)$  in the SSH model experience a sudden change during the quench, which leads to the pre- and post-quenched Bloch vectors  $\mathbf{d}(k) = (J_0, 0, 0)$  and  $\mathbf{d}'(k) =$

$[J_1 + J_0 \cos(k), J_0 \sin(k), 0]$ , respectively. With the K-theory classification of quench dynamics, the parent Bloch Hamiltonian reads  $H(t, k) = \mathbf{d}(t, k) \cdot \boldsymbol{\sigma}$ , where the components of  $\mathbf{d}(t, k)$  are given by [31]  $d_x(t, k) = -J_0 + 2J_0 [J_0 \sin(k) \chi(t, k)]^2$ ,  $d_y(t, k) = -2J_0^2 [J_1 + J_0 \cos(k)] \sin(k) \chi(t, k)^2$ , and  $d_z(t, k) = -J_0^2 \sin(k) \sin[2d'(k)t] / d'(k)$ , respectively, where  $d'(k)$  is the norm of  $\mathbf{d}'(k)$ ,  $\chi(t, k) = \sin[d'(k)t] / d'(k)$  and  $(t, k) \in [0, \pi/d'(k)] \times [0, \pi]$ . The same learning protocol as above can be used to learn the phase transition in  $(J_0, J_1)$  space, and shown in Fig. 4(a) is the retrieved critical line (blue stars), which fits the theoretical result (dashed blue line) well. The dynamical topological numbers  $\mathcal{C}$  in each sector are calculated with the method provided in Ref. [31]. Figure 4(b) shows that there are two topological sectors in the phase diagram (we have taken  $t = 100$ ). Figure 4(c) displays the diffusion-space distribution of uniformly sampled  $M = 1000$  data points from  $J_1 = 0$  to  $J_1 = 2J_0$  with  $J_0 = 1$ . The color code indicates the value of  $J_1/J_0$ . The  $k$ -means clustering method is used in this low-dimensional Euclidean space to learn the critical line automatically.

*Discussion.*—While the ED may, in simple cases and for fine-tuned choices of  $\epsilon$ , deliver correct clustering, the CD is much more consistent and generic in its performance. This is because it naturally exploits the characteristic features of TQPTs. Moreover, it is inspired by manifold learning, where the Euclidean similarity measure may fail in general. The  $\mathbb{L}^\infty$ -norm distance metric approximately captures the features of TQPTs for states in momentum space. Based on the mathematical fact that the Fourier transform of a  $\mathbb{L}^1(\mathbb{R})$  space is the  $\mathbb{L}^\infty(\mathbb{R})$  space, the corresponding dual distance metric in real space could be given by the  $\mathbb{L}^1$ -norm. Future di-

rections include considering quantum speedups for these methods [24, 45–49], and applications in other topological quantum systems [50–57].

*Summary.*—In summary, we have proposed to use the  $\mathbb{L}^\infty$ -norm as an approximative topological distance measure in momentum space, and to use manifold learning to retrieve TQPTs. The Chebyshev distance in general captures the relevant similarities and differences between topological states defined on the compact BZ. In the examples considered, the critical lines in the phase diagrams were precisely identified without pre-training. Our work thus paves the way toward automatic detections of topological phase diagrams without prior analysis of the Hamiltonian.

*Note added.*—After this work was completed, two related preprints [58, 59] appeared, studying unsupervised clustering of topological states using different distance metrics and with different emphases compared to our work.

*Acknowledgments.*—We acknowledge helpful discussions with Yu-Ran Zhang and Zhengyang Zhou. T.L. acknowledges support from the Grant-in-Aid for a JSPS Foreign Postdoctoral Fellowship (P18023). F.N. is supported in part by the: MURI Center for Dynamic Magneto-Optics via the Air Force Office of Scientific Research (AFOSR) (FA9550-14-1-0040), Army Research Office (ARO) (Grant No. Grant No. W911NF-18-1-0358), Japan Science and Technology Agency (JST) (via the Q-LEAP program, and the CREST Grant No. JP-MJCR1676), Japan Society for the Promotion of Science (JSPS) (JSPS-RFBR Grant No. 17-52-50023, and JSPS-FWO Grant No. VS.059.18N), the RIKEN-AIST Challenge Research Fund, the Foundational Questions Institute (FQXi), and the NTT PHI Laboratory.

---

\* yanmingche01@gmail.com

† fnori@riken.jp

- [1] M. Z. Hasan and C. L. Kane, “Colloquium: Topological insulators,” *Rev. Mod. Phys.* **82**, 3045–3067 (2010).
- [2] X.-L. Qi and S.-C. Zhang, “Topological insulators and superconductors,” *Rev. Mod. Phys.* **83**, 1057–1110 (2011).
- [3] S. H. Mousavi, A. B. Khanikaev, and Z. Wang, “Topologically protected elastic waves in phononic metamaterials,” *Nat. Commun.* **6**, 1 (2015).
- [4] Y. Liu, Y. Xu, S.-C. Zhang, and W. Duan, “Model for topological phononics and phonon diode,” *Phys. Rev. B* **96**, 064106 (2017).
- [5] T. Ozawa, H. M. Price, A. Amo, N. Goldman, M. Hafezi, L. Lu, M. C. Rechtsman, D. Schuster, J. Simon, O. Zilberman, and I. Carusotto, “Topological photonics,” *Rev. Mod. Phys.* **91**, 015006 (2019).
- [6] M. Klintenberg, J. T. Haraldsen, and A. V. Balatsky, “Computational search for strong topological insulators: An exercise in data mining and electronic structure,” *Applied Physics Research* **6**, 4 (2014).
- [7] P. Zhang, H. Shen, and H. Zhai, “Machine learning topological invariants with neural networks,” *Phys. Rev. Lett.* **120**, 066401 (2018).
- [8] N. Sun, J. Yi, P. Zhang, H. Shen, and H. Zhai, “Deep learning topological invariants of band insulators,” *Phys. Rev. B* **98**, 085402 (2018).
- [9] P. Huembeli, A. Dauphin, and P. Wittek, “Identifying quantum phase transitions with adversarial neural networks,” *Phys. Rev. B* **97**, 134109 (2018).
- [10] N. Yoshioka, Y. Akagi, and H. Katsura, “Learning disordered topological phases by statistical recovery of symmetry,” *Phys. Rev. B* **97**, 205110 (2018).
- [11] L. Pilozzi, F. A. Farrelly, G. Marcucci, and C. Conti, “Machine learning inverse problem for topological photonics,” *Commun. Phys.* **1**, 1 (2018).
- [12] J. F. Rodriguez-Nieva and M. S. Scheurer, “Identifying topological order through unsupervised machine learning,” *Nat. Phys.* **15**, 790–795 (2019).
- [13] E. Greplova, A. Valenti, G. Boschung, F. Schäfer, N. Lörch, and S. Huber, “Unsupervised identification of topological order using predictive models,” *arxiv:1910.10124* (2019).
- [14] G. Carleo, I. Cirac, K. Cranmer, L. Daudet, M. Schuld, N. Tishby, L. Vogt-Maranto, and L. Zdeborová, “Machine learning and the physical sciences,” *Rev. Mod. Phys.* **91**, 045002 (2019).
- [15] L. Wang, “Discovering phase transitions with unsupervised learning,” *Phys. Rev. B* **94**, 195105 (2016).
- [16] G. Carleo and M. Troyer, “Solving the quantum many-body problem with artificial neural networks,” *Science* **355**, 602–606 (2017).
- [17] E. P. L. Van Nieuwenburg, Y.-H. Liu, and S. D. Huber, “Learning phase transitions by confusion,” *Nat. Phys.* **13**, 435 (2017).
- [18] J. Carrasquilla and R. G. Melko, “Machine learning phases of matter,” *Nat. Phys.* **13**, 431 (2017).
- [19] Y.-H. Liu and E. P. L. van Nieuwenburg, “Discriminative cooperative networks for detecting phase transitions,” *Phys. Rev. Lett.* **120**, 176401 (2018).
- [20] W.-J. Rao, Z. Li, Q. Zhu, M. Luo, and X. Wan, “Identifying product order with restricted Boltzmann machines,” *Phys. Rev. B* **97**, 094207 (2018).
- [21] K. Ch’ng, N. Vazquez, and E. Khatami, “Unsupervised machine learning account of magnetic transitions in the Hubbard model,” *Phys. Rev. E* **97**, 013306 (2018).
- [22] S. Durr and S. Chakravarty, “Unsupervised learning eigenstate phases of matter,” *Phys. Rev. B* **100**, 075102 (2019).
- [23] Y. Ming, C.-T. Lin, S. D. Bartlett, and W.-W. Zhang, “Quantum topology identification with deep neural networks and quantum walks,” *npj Computational Materials* **5**, 1–7 (2019).
- [24] P. Mehta, M. Bukov, C.-H. Wang, A. G.R. Day, C. Richardson, C. K. Fisher, and D. J. Schwab, “A high-bias, low-variance introduction to machine learning for physicists,” *Physics Reports* **810**, 1–124 (2019).
- [25] Humberto Munoz-Bauza, Firas Hamze, and Helmut G. Katzgraber, “Learning to find order in disorder,” *arxiv:1903.06993* (2019).
- [26] K. Fukushima, S. S. Funai, and H. Iida, “Featuring the topology with the unsupervised machine learning,” *arxiv:1908.00281* (2019).
- [27] J. B. Tenenbaum, V. De Silva, and J. C. Langford, “A global geometric framework for nonlinear dimensionality reduction,” *Science* **290**, 2319–2323 (2000).

[28] R. R. Coifman, S. Lafon, A. B. Lee, M. Maggioni, B. Nadler, F. Warner, and S. W. Zucker, “Geometric diffusions as a tool for harmonic analysis and structure definition of data: Diffusion maps,” *Proc. Natl. Acad. Sci. U.S.A.* **102**, 7426–7431 (2005).

[29] R. R. Coifman and S. Lafon, “Diffusion maps,” *Appl. Comput. Harmon. Anal.* **21**, 5–30 (2006).

[30] X.-L. Qi, Y.-S. Wu, and S.-C. Zhang, “Topological quantization of the spin Hall effect in two-dimensional paramagnetic semiconductors,” *Phys. Rev. B* **74**, 085308 (2006).

[31] Z. Gong and M. Ueda, “Topological entanglement-spectrum crossing in quench dynamics,” *Phys. Rev. Lett.* **121**, 250601 (2018).

[32] S. T. Roweis and L. K. Saul, “Nonlinear dimensionality reduction by locally linear embedding,” *Science* **290**, 2323–2326 (2000).

[33] E. Macías-Virgós and D. Mosquera-Lois, “Homotopic distance between maps,” [arxiv:1810.12591](https://arxiv.org/abs/1810.12591) (2018).

[34] Take, for instance, the normalized Bloch vector  $\hat{\mathbf{d}}$  in the SSH model at  $k = \pi$  in the BZ, which transforms from  $(1, 0, 0)$  to  $(-1, 0, 0)$  across the topological phase transition. See the SSH Hamiltonian in the main text.

[35] Note that here the distances are normalized:  $\mathcal{K}_{ij}^\infty = \exp(-\|\mathbf{x}_i - \mathbf{x}_j\|_{\mathbb{L}^\infty}^2/4\epsilon)$  and  $\mathcal{K}_{ij}^{p=2} = \exp[-\|\mathbf{x}_i - \mathbf{x}_j\|_{\mathbb{L}^2}^2/4\epsilon(N+1)^{2D}]$ , where the BZ is sliced into  $N^D$  patches in the  $D$ -dimensional case. It can be shown that  $\mathcal{K}_{ij}^{p=2} \geq \mathcal{K}_{ij}^\infty$  for the same  $\epsilon$ . We find that for the same  $\epsilon$ , the ED overestimates the inter-cluster connections as compared to the CD, and fails to detect certain topological transitions.

[36] L. van der Maaten and G. Hinton, “Visualizing data using t-SNE,” *Journal of machine learning research* **9**, 2579–2605 (2008).

[37] M. Belkin and P. Niyogi, “Laplacian eigenmaps and spectral techniques for embedding and clustering,” in *Advances in neural information processing systems* (2002) pp. 585–591.

[38] M. Belkin and P. Niyogi, “Laplacian eigenmaps for dimensionality reduction and data representation,” *Neural computation* **15**, 1373–1396 (2003).

[39] B. Nadler, S. Lafon, I. Kevrekidis, and R. R. Coifman, “Diffusion maps, spectral clustering and eigenfunctions of Fokker-Planck operators,” in *Advances in neural information processing systems* (2006) pp. 955–962.

[40] Z. Farbman, R. Fattal, and D. Lischinski, “Diffusion maps for edge-aware image editing,” *ACM Transactions on Graphics (TOG)* **29**, 145 (2010).

[41] L. Haghverdi, F. Buetner, and F. J. Theis, “Diffusion maps for high-dimensional single-cell analysis of differentiation data,” *Bioinformatics* **31**, 2989–2998 (2015).

[42] Note that the eigenvalues of the probability matrix  $P$  satisfy  $0 \leq \lambda_i \leq 1$ . Hence when the number of diffusion steps  $t$  is large, the nontrivial dimensions are given by  $\lambda_i \approx 1$  and the corresponding degree of degeneracy corresponds to the effective dimension of the  $Y$  space, and also is the number of connected components in the similarity ma-

trix [12]. The first eigenvector is  $\psi_0 \propto 1/M = \text{const}$ , so data images are not fully dispersed in this dimension.

[43] W. P. Su, J. R. Schrieffer, and A. J. Heeger, “Soliton excitations in polyacetylene,” *Phys. Rev. B* **22**, 2099–2111 (1980).

[44] J. K. Asbóth, L. Oroszlány, and A. Pályi, *A Short Course on Topological Insulators* (Springer International Publishing, 2016).

[45] M. Schuld, I. Sinayskiy, and F. Petruccione, “An introduction to quantum machine learning,” *Contemp. Phys.* **56**, 172–185 (2014).

[46] R. Chatterjee and T. Yu, “Generalized coherent states, reproducing kernels, and quantum support vector machines,” *Quantum Inf. Commun.* **17**, 1292 (2017).

[47] J. Biamonte, P. Wittek, N. Pancotti, P. Rebentrost, N. Wiebe, and S. Lloyd, “Quantum machine learning,” *Nature* **549**, 195–202 (2017).

[48] M. Schuld, M. Fingerhuth, and F. Petruccione, “Implementing a distance-based classifier with a quantum interference circuit,” *EPL* **119**, 60002 (2017).

[49] V. Dunjko and H. J. Briegel, “Machine learning & artificial intelligence in the quantum domain: a review of recent progress,” *Reports on Progress in Physics* **81**, 074001 (2018).

[50] S. Malzard, C. Poli, and H. Schomerus, “Topologically protected defect states in open photonic systems with non-hermitian charge-conjugation and parity-time symmetry,” *Phys. Rev. Lett.* **115**, 200402 (2015).

[51] Y.-R. Zhang, Y. Zeng, H. Fan, J. Q. You, and F. Nori, “Characterization of topological states via dual multipartite entanglement,” *Phys. Rev. Lett.* **120**, 250501 (2018).

[52] F. Schindler, A. M. Cook, M. G. Vergniory, Z. Wang, S. S. P. Parkin, B. A. Bernevig, and T. Neupert, “Higher-order topological insulators,” *Science Advances* **4**, eaat0346 (2018).

[53] Zhongbo Yan, Fei Song, and Zhong Wang, “Majorana corner modes in a high-temperature platform,” *Phys. Rev. Lett.* **121**, 096803 (2018).

[54] T. Liu, J. J. He, and F. Nori, “Majorana corner states in a two-dimensional magnetic topological insulator on a high-temperature superconductor,” *Phys. Rev. B* **98**, 245413 (2018).

[55] D. Leykam, K. Y. Bliokh, C. Huang, Y. D. Chong, and F. Nori, “Edge modes, degeneracies, and topological numbers in non-hermitian systems,” *Phys. Rev. Lett.* **118**, 040401 (2017).

[56] T. Liu, Y.-R. Zhang, Q. Ai, Z. Gong, K. Kawabata, M. Ueda, and F. Nori, “Second-order topological phases in non-hermitian systems,” *Phys. Rev. Lett.* **122**, 076801 (2019).

[57] K. Y. Bliokh, D. Leykam, M. Lein, and F. Nori, “Topological non-hermitian origin of surface Maxwell waves,” *Nat. Commun.* **10**, 1 (2019).

[58] M. S. Scheurer and R.-J. Slager, “Unsupervised machine learning and band topology,” [arxiv:2001.01711](https://arxiv.org/abs/2001.01711) (2020).

[59] Y. Long, J. Ren, and H. Chen, “Unsupervised manifold clustering of topological phononics,” [arxiv:2001.02661](https://arxiv.org/abs/2001.02661) (2020).